Determination of *h*/*e* from the Photoelectric Effect

Brian Lim and P. McEuen

Cornell University, Ithaca, NY 14853, USA

(received 9 December 2005)

By measuring the current generated in a photomultiplier tube (PMT), due to exposure from various frequencies the mercury arc, the photoelectric effect was observed. By varying the applied voltage and studying the subsequent I-V curves of the PMT, the stopping voltages of the generated photoelectrons are estimated, using linear approximations. Comparing the stopping voltages against frequency, h/e = $3.4 \pm 0.3 \times 10^{-15}$ Vs is determined within 18% from the accepted value of 4.136×10^{-15} Vs. Alternative methods to estimate stopping voltages are also briefly investigated and evaluated.

1. Introduction

One of the major break throughs by Einstein in his pivotal 1905 papers, the photoelectric effect[1] helped to solidify the notion of light as quanta. Drawing from Planck's quantum hypothesis for blackbody radiation, that light has energy quanta $E = hf$, Einstein extended it to explain how the interaction of light with electrons of a metal give rise to photoelectrons. His photoelectric theory explains why and how the velocity of the electrons, and thus the measured voltage, varies with frequency and not light intensity. The latter affects the current of the electrons in this quantum theory, which is much contrary to the wave nature of light much accepted since Young's double slit experiment. First demonstrated successfully by Milikan[2], the photoelectric experiment has become a staple in advanced undergraduate physics labs, using more advanced equipment, with the primary goal

of determining the ratio of Planck's constant, h, against the electron charge, e, i.e. h/e, while revealing the intricacies involved in obtaining the results.

2. Description of Apparatus

The experimental set-up (Figure 2.1) comprises (*a*) a mercury lamp (with a General Electric H100-A4/T 100W mercury bulb), to emit photons of specific frequencies, (*b*) a Hamamatsu photomultiplier tube 1P28 to generate photoelectrons, and (*c*) a disc, placed in front of the PMT with 5 filters: yellow, green, blue, violet, and ultraviolet. With these filters in front of the mercury source, the respective wavelengths, 5780A, 5461A, 4358A, 4047A, 3663A, are obtained. Current is measured with the Keithley 480 Picoammeter, and voltage with the Fluke 77 Multimeter. A black cloth is draped over the apparatus to reduce background light exposure.

When conducting the experiment, it is best to have all the maximum forward currents equal to give the same normalization factor. Assuming that the magnitude of the current is directly proportional to the light intensity, the position of the mercury lamp, with respect to the PMT, is

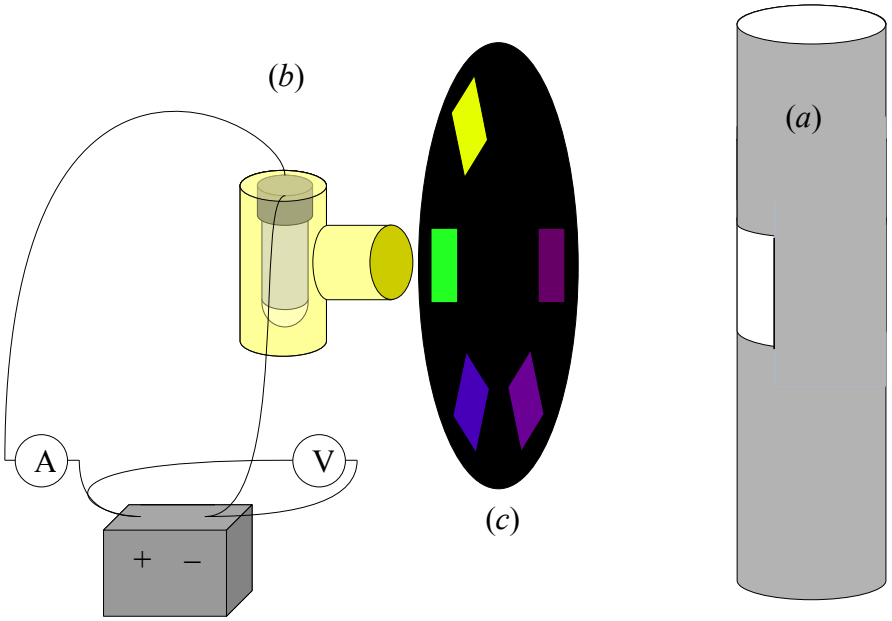

Figure 2.1: Apparatus set-up. The mercury source intensity can be adjusted by moving the lamp nearer/farther from the detector, or changing the angle of light incidence.

adjusted to provide equal intensity. This is to compensate for the nonlinearity of the intensity of each frequency of the mercury spectrum (Figure 2.2), and the nonlinear spectral response of the PMT[3]. Unfortunately, this adjustment was done crudely by merely shifting the retort stand that supports the lamp until the current reading from the PMT is equal for the maximum forward currents.

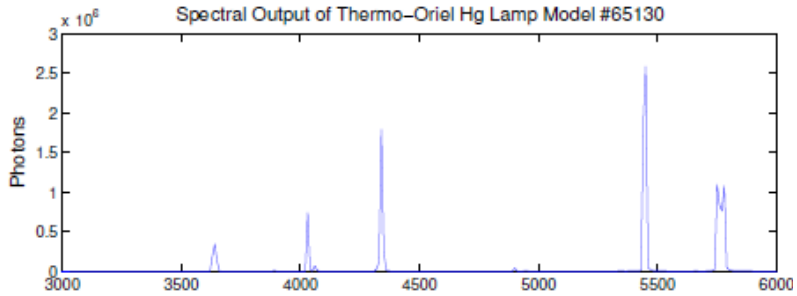

Figure 2.2: An example of the nonlinear intensity distribution of the mercury spectrum. Src: http://ocw.mit.edu/NR/rdonlyres/Physics/8-13-14Fall-2004-Spring-2005/A0478CD2-2136-4FA4-8EDC-85065AB6C2C1/0/jlexp002.pdf

Furthermore, this calibration has to be repeated during the course of the experiment, due to a persistent drift of the maximum forward current. For the yellow and violet fequencies, with the weakest detection rates, the most profound drifting is observed, as the lamp is situated closest to filters and detector, causing their significant heating. The drifting is reduced a little when the lamp is brought farther away from the detector, but this compromises the requirement of maintaining a constant normalization factor of maximum forward current for all frequencies. Therefore, only the yellow frequency has a low current intensity, while the other frequencies are equally high. However, even with these measures, the drift is noticeable and causes the most significant of errors for this experiment.

3. Theory

The photoelectric effect involves the absorption of energy from a photon, $E = hf$, by an electron, such that the latter has sufficient energy to escape the metal surface of the cathode. Depending on the original energy of the electron in the metal, part of the photon energy goes into the work

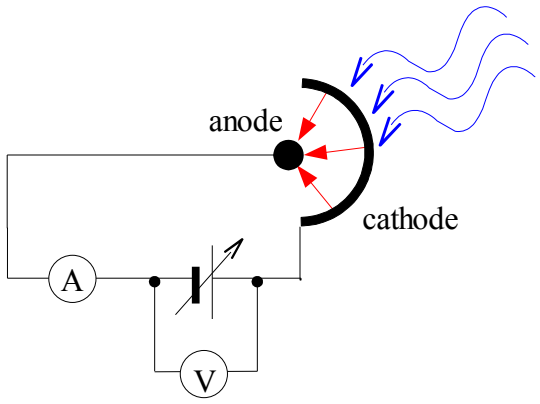

Figure 3.1: Circuit schematic of apparatus

function ϕ , while the remainder contributes to its kinetic energy. Thus derives the famous equation by Einstein:

$$eV = \frac{1}{2} m_e v^2 = h f - \phi \,, \tag{3.1}$$

where the energy of the electron can also be represented as eV, the electron charge multiplied by its voltage. Figure 3.1 illustrates the generation of photoelectrons from illumination.

Of the electrons that escape, there is a maximum velocity which can be determined in terms of voltage. By applying a potential difference across the cathode and anode, opposing the electron path, the flow of photoelectrons can be made to stop. The stopping voltage, at which this just happens, can be used to calculate the ratio h/e, by the equation

$$V_s = \frac{h}{e} f - \frac{\phi_m}{e} \,. \tag{3.2}$$

The distribution of energy of the electrons in the metal surface can be explained using quantum mechanics and Fermi statistics[4]. Being Fermi particles, electrons follow the Fermi-Dirac distribution[5]

$$n(k) = \frac{1}{e^{(\varepsilon(k)-\mu)/k_B T} + 1}$$

which describes the average number of electrons distributed by their wavenumber, k, where $\varepsilon(k)$ is the

electron energy, μ is the chemical potential at that state, k_B is the Boltzmann constant, and T is the temperature. In terms of energy, the density of states in 3D for a free particle is $D(\varepsilon) \sim \sqrt{\varepsilon}$ [6], giving the distribution of energy as

$$n(\varepsilon) \sim \int_0^{\varepsilon} \frac{\sqrt{\varepsilon}}{e^{(\varepsilon-\mu)/k_B T}+1} d\varepsilon \,. \tag{3.3}$$

The integrand in Equation 3.3 is plotted in Figure 3.2. Since $\varepsilon \sim V$ and $f \sim I$, the I-V curve should follow Equation 3.3, and its derivative dI/dV vs. V should resemble Figure 3.3, within the validity of the assumptions.

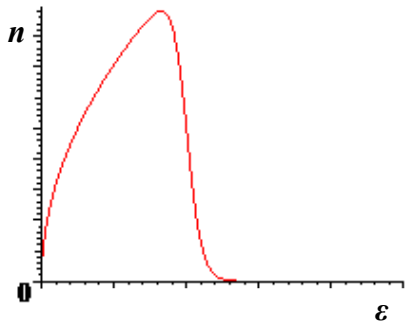

Figure 3.3: Distribution of energies for free particles

Figure 3.4 shows an energy level view[7] of how the energy of an absorbed photon shifts the energy of a free electron in an Fermi sea (metal surface, for this case). Part of the energy hf is used to raise the electron energy above the Fermi energy, E_F, while the remainder contributes to its kinetic energy.

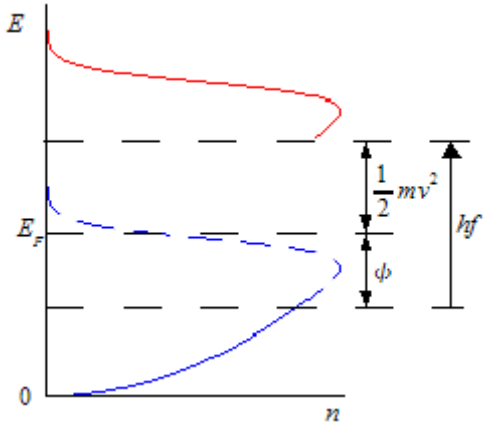

Figure 3.4: Energy level representation of free electron excitation from a photon

Thus, depending on the frequency of light used, the distribution of kinetic energies of the electrons would be different.

4. Determination of the Stopping Voltages

Currently, the method of obtaining the stopping voltages from the I-V curves of photoelectron detectors is much of an art. This section describes popular techniques mentioned by Hughes and DuBridge[8], Hall and Tuttle[9], and Wright[10].

When a retarding potential is applied against the photoelectrons, fewer of them reach the anode and the current diminishes. For large positive voltages, the current is constant as the maximum number of photoelectrons have been produced. When the current reaches zero, the most energetic electrons have been turned away from the anode. This ideal behavior is described by the curve *abcd* in Figure 4.1. However, the characteristics of the apparatus poses some problems, and lead to distortions.

Since different metals are used for anode and cathode, to reduce reverse current, there is a nonzero contact potential, thus the curve is shifted to *abefd*. Notice that the position of the *V*-intercept is not changed by much. However, not all of the reverse current can be eliminated. This reverse current arises when electrons escaping from the anode (instead of the cathode), due to photoelectric emission on exposure to light, or thermionic emission, due to heat. With the reverse

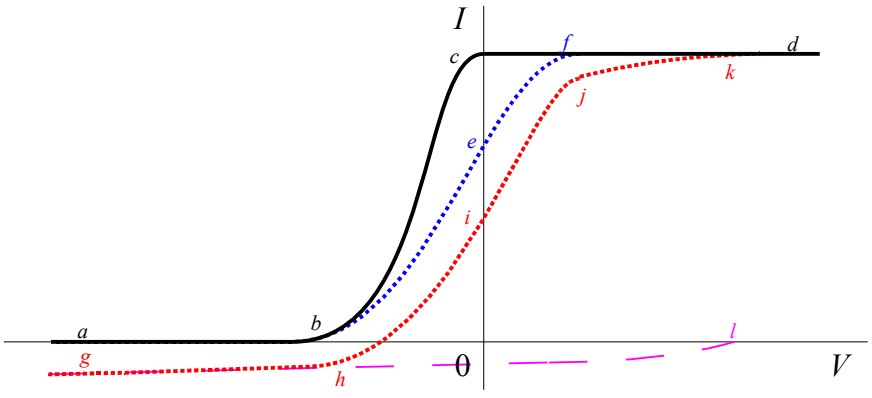

Figure 4.1: Original curve (abcd) distorted due to contact potential (effect abefd) and also reverse current (ghl) to give final curve (ghijkd). Adapted from Hughes and DuBridge[8]

current of curve *ghl*, the I-V curve is lowered to *ghijkd*. In this experiment, only the stopping voltages are of importance and not the overall shape of the I-V curve. To attempt to recover the curve *abefd*, the reverse current, *ghl*, should be estimated and subtracted off *ghijkd*. Hughes and DuBridge[8], Hall and Tuttle[9], and Wright[10] also describe the functional, yet unscientific, technique of plotting $\sqrt{I}$ vs V, that provides a straight line in the region *be* to which a linear fit can be made to determine the V-intercept stopping potential.

5. Data and Data Analysis

Four sets of data were compiled with the final set presented in Appendix B. This set consists of results recorded over two days (18th and 20th Nov 2005), of which there are slight discrepancies between data recorded in each day, due to significant calibration drift. After some careful corrections and re-normalizations to reduce the systematic drift errors, the data is plotted in Figure 5.1, to show the I-V characteristic of the PMT for the five available filters.

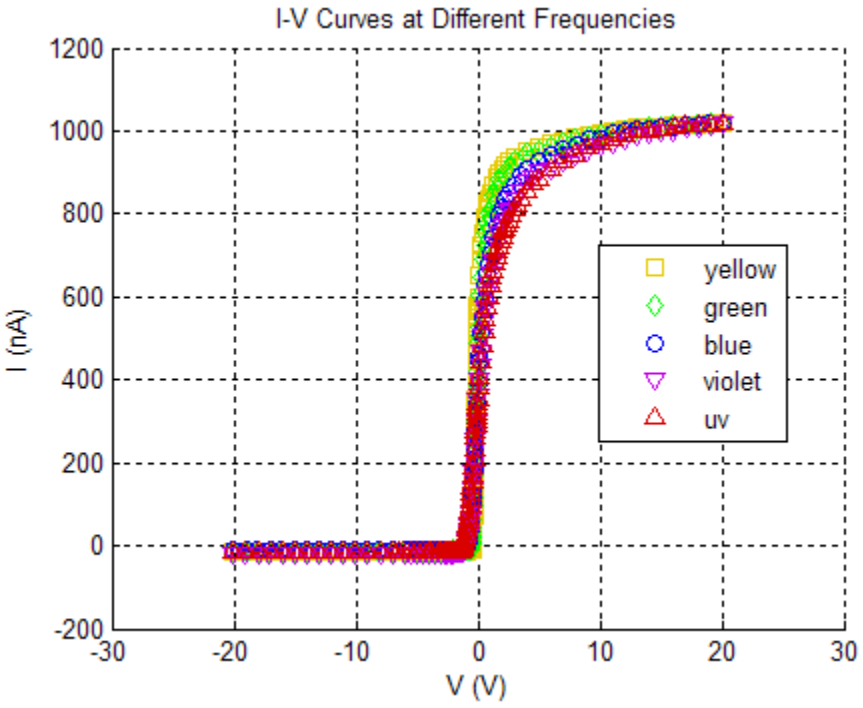

Figure 5.1: Scaled I-V charateristics for various colors of light incident on the PMT. Compare with curve abcde in Figure 4.1.

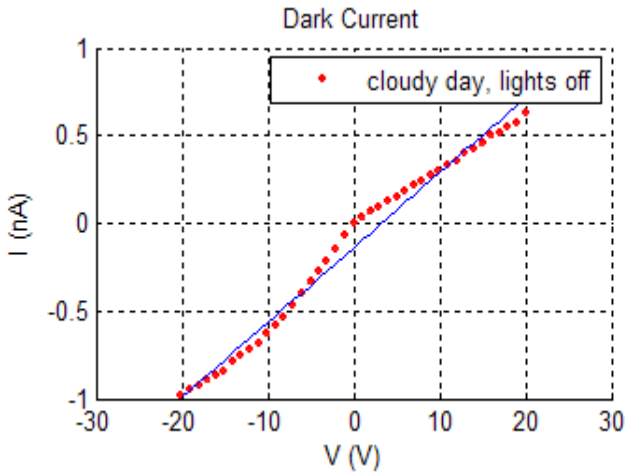

Figure 5.2: Dark current measured when the PMT is totally covered by a black cloth, in a room with lights off, on a rainy day. A linear approximation is calculated and used to compute its contribution to the error in I.

Most of this data set was collected under low light conditions in a room without lights and with an uncovered window, either after dark or with a overcast sky with dim daylight. However, even with the mercury lamp turned off, and the PMT totally covered by a the opaque part of the filter disc, and a black cloth, a dark current is still noticeable. The dark current for the worst-case, brightest environment (see Figure 5.2), is considered for its contribution to the error in measuring *I*. The magnitude of the dark current enforces the positioning of the mercury lamp close enough to the PMT to provide a high enough maximum forward current to minimize its effects.

The biggest contribution to the error, though, is the aforementioned "calibration drift". For every few readings, the maximum forward current is checked to determine how much it has drifted, especially for the yellow frequency. Readjusting the lamp reduces the drift, and from how often this has to be done, a vague notion of the drift error is estimated. It is presented in Table 5.1. Combined with the intrinsic errors of using the picoammeter and multimeter, the total errors are estimated.

Working in normalized currents, $J = I / I_0$, where I_0 is the maximum forward current for

	Yellow	***Green***	***Blue***	***Violet***	***UV***
Drift Error (nA)	10	3	1	4	3.5

Table 5.1: Very rough estimates of the drift errors for each measurement at the particular frequencies.

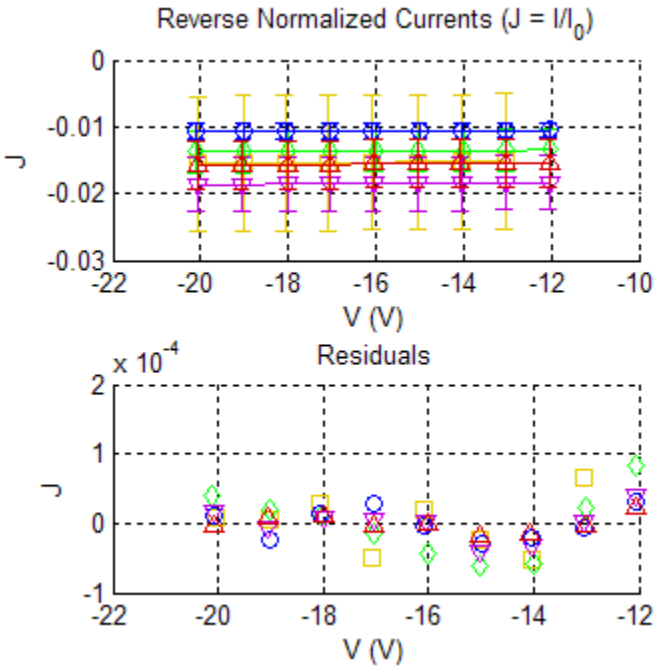

Figure 5.3: Reverse currents, linearly fitted

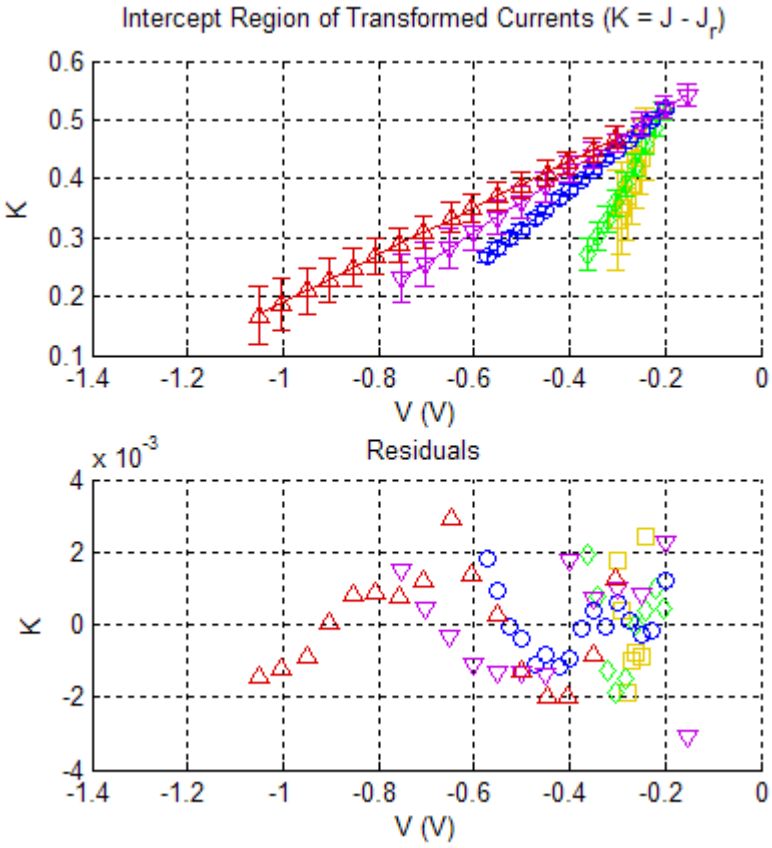

Figure 5.4: Linear fitting of region in K near V_S

each frequency, the reverse currents J_r are linearly fitted (using the method detailed in Appendix A) to $J_r^{(fit)} = A_r + B_r V$ (Figure 5.3) and subtracted from J. It is noticed that the nearer the mercury lamp was placed to the PMT, the larger the magnitude of J_r; Figure 5.3 shows that the lamp was nearest for violet light and farthest for blue. Using the technique recommended by Hughes and DuBridge[8], Hall and Tuttle[9], and Wright[10], the quantity

$$K = \sqrt{J - J_r^{(fit)}} \tag{5.1}$$

is plotted against V, to produce nearly straight lines near the V-intercepts (Figure 5.4). This is fit linearly as

$$K^{(fit)} = A_K + B_K V . \tag{5.2}$$

From the V-intercept of Equation 5.2, the stopping voltage is

$$V_s = -(-A_K / B_K) \tag{5.3}$$

Figure 5.5 plots each V_S corresponding to its frequency, f, and conducts a fit according to Equation 3.2.

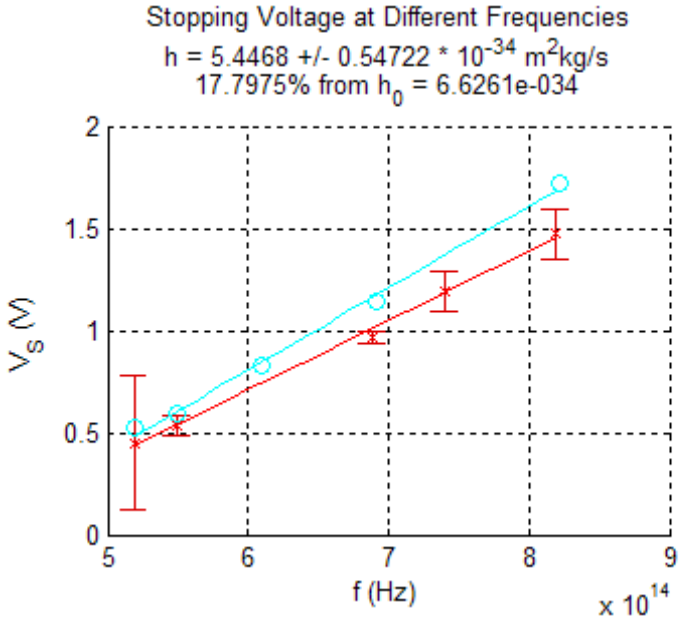

Figure 5.5: Determination of the ratio h/e from stopping voltages. The large error in the yellow (lowest) frequency is due to the severe calibration drift for that color. The upper plot shows results from Hall and Tuttle[9] included for comparison.

From quadrature, the errors in J and J_r are calculated as

$$\delta J = \sqrt{\left(\frac{\delta I}{I_0}\right)^2 + \left(-\frac{I}{I_0^2}\delta I_0\right)^2} = \frac{1}{I_0}\sqrt{(\delta I)^2 + \left(\frac{I}{I_0}\delta I_0\right)^2} \tag{5.4}$$

Using Appendix A, the uncertainties in the coefficients of $J_r^{(fit)}$ are determined and used to determine

$$\delta J_r^{(fit)} = \sqrt{\left(\delta A_r\right)^2 + \left(V\,\delta B_r\right)^2 + \left(B_r\,\delta V\right)^2}\,. \tag{5.5}$$

The error in K is

$$\delta K = \frac{1}{2K}\sqrt{\left(\delta J\right)^2 + \left(-\delta J_r^{(fit)}\right)^2}\,, \tag{5.6}$$

which is used to provide the weights for the weighted linear least squares for $K^{(fit)}$. Having worked out, via Appendix A, the errors in the coefficients of $\delta K^{(fit)}$, the error in V_S is

$$\delta V_s = \sqrt{\left(\frac{-A_K\,\delta B_K}{B_K^2}\right)^2 + \left(\frac{\delta A_K}{B_K}\right)^2}\,. \tag{5.7}$$

Finally, from Equation 3.2 and Appendix A, the error in h/e, is $\delta(h/e) = \delta B$. With all the values computed via Matlab, the ratio is found to be $h/e = 3.4 \pm 0.3 \times 10^{-15}\,\text{Vs}$. This result is 18% off from the accepted value of $h/e = (6.626 \times 10^{-34}\,\text{Js})/(1.602 \times 10^{-19}\,\text{C}) = 4.136 \times 10^{-15}\,\text{Vs}$. The latter value also lies outside the range of error for this experiment, suggesting that the set-up and/or procedure is not good enough to provide accurate results.

6. Alternative Methods of Determining Stopping Voltages

The previous analysis has been used to determine the h/e ratio, because of its simplicity and popularity[8,9,10]. However, other more esoteric schemes have been explored.

Instead of doing linear fits on the data at the reverse current and intercept regions, nonlinear

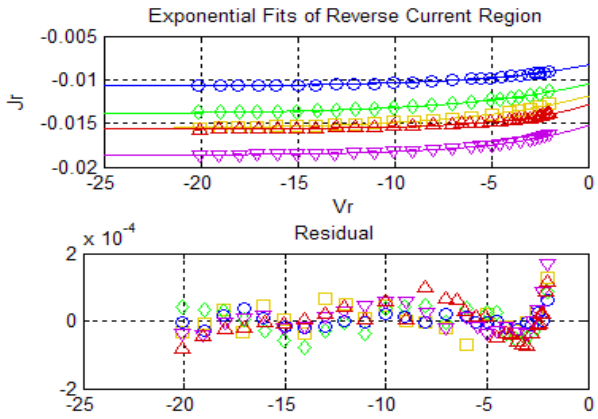

Figure 6.1: Exponential fit of the reverse currents

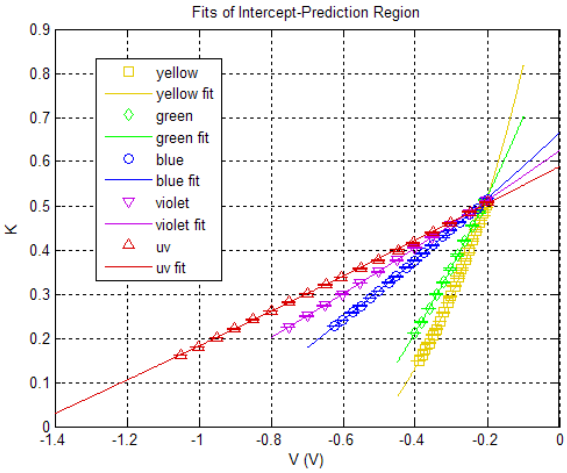

Figure 6.2: Exponential fit of the intercept region

exponential fits of the form $a_r e^{b_r V} - c_r$ is used (Figure 6.1, 6.2). This gives smaller residuals for wider ranges, but have uncertainties in the parameters too large that it defeats using this technique. With this, h/e was calculated to be $h/e = 3 \pm 7 \times 10^{-15}$ Vs , which is unacceptable.

Another analysis involves looking at the difference between adjacent plots to give the derivative plot dI/dV vs V , in an attempt to verify the theory described in at the end of Section 3, about the Fermi-Dirac distribution. Unfortunately, as Figure 6.3 shows, the graphs do not behave as expected: the peaks are all almost aligned, and the widths increase with increasing frequency. Probably, because

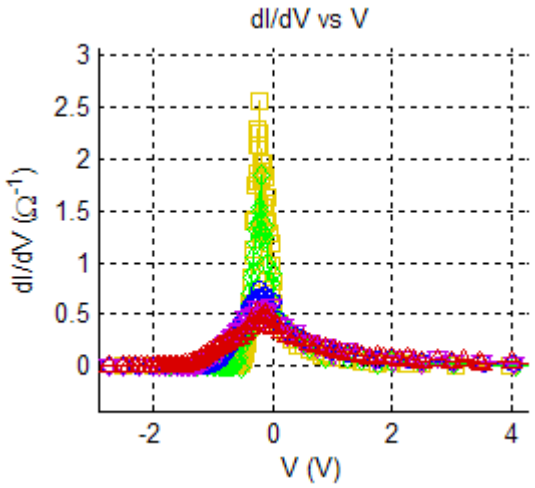

Figure 6.3: Plot of adjacent difference in I divided by the adjacent difference in V against V. Compare with Figure 3.3 to see that the two are not similar.

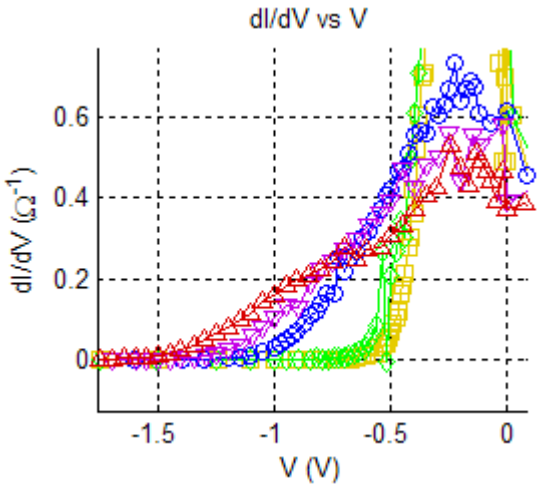

Figure 6.4: Exponential fit of the reverse currents

the electrons are not truly free. However, on closer inspection, the intercept region (which are about half of the original analysis) of this graph is also almost linear. This suggests the use of linear fits to obtain the V-intercepts to determine V_S may be feasible. But given the complexity and lack of use of this method, it is unfavorable.

8. Conclusion

The simple experiment of using a retarding potential to investigate photoelectrons to find the h/e ratio has given rise to the value $3.4 \pm 0.3 \times 10^{-15}$ Vs which is too far from the accepted value of 4.136×10^{-15} Vs . However, historically, there have been experiments[9,10,11] conducted in a similar manner that have given much more accurate results, even though the technology used here, such as the PMT, did not exist then. This suggests that much has to be done to control the experimental conditions to further reduce errors, especially the calibration drift. Also, it was also realized that the theory for the photoelectric effect could still be much more thoroughly investigated to explain the results discussed regarding the nonlinear behavior of the I-V characteristics. Even with the improvements in error

reduction, it seems that this classical approach to determining *h*/*e* using the photoelectric effect, though simple, is prone to systematic errors.

Acknowledgements

My appreciation goes out to Prof McEuen for his guidance, and patience in answering the many questions I had, and Prof Joel Brock for his pointing out the Fermi-Dirac distribution of the photoelectrons and how photon excitation affects it.

References

1. A. Einstein, Ann. d. Phys. **17**, 132 (1905).
2. R. A. Millikan, Phys. Rev. 7, 355 (1916).
3. Datasheet for Hamamatsu Photonics K.K., Photomultiplier Tube 1P28. Retrieved from http://sales.hamamatsu.com/assets/pdf/parts_misc/1P28.pdf on 4th December 2005.
4. F. K. Richtmyer, E. H. Kennard, *Introduction to Modern Physics*, 4E, McGraw-Hill, New York, 1947, Sec 51-52, 56, p91-94, 100-103.
5. R. Bowley, M. Sánchez, *Introductory Statistical Mechanics*, 2E, Oxford Science Publications, 2004, Sec 10.2-10.3, p212-216.
6. R. Bowley, M. Sánchez, *Introductory Statistical Mechanics*, 2E, Oxford Science Publications, 2004, Sec 7.3, p150-151.
7. J. D. Brock, private communication.
8. A. L. Hughes, L. A. DuBridge, *Photoelectric Phenomena*, McGraw-Hill, New York, 1932, Ch1-2, p1-37.

9. H. H. Hall, R. P. Tuttle, Am. Jour. Phys. **59**, 50 (1970).

10. W. R. Wright, American Physics Teacher (Am. Jour. Phys.) **5**, 65 (1937).

11. A. C. Melissinos, Experiments in Modern Physics, Academic Press, 1966, ch1, p18-27.